Spatial and Orientational Structure of the Hydration Shell of Benzene in Sub- and Supercritical Water

ARTICLE *in* THE JOURNAL OF PHYSICAL CHEMISTRY B · JUNE 2015

Impact Factor: 3.3 · DOI: 10.1021/acs.jpcb.5b03371 · Source: PubMed

2 AUTHORS, INCLUDING:

Ashu Choudhary

Indian Institute of Technology Kanpur

3 PUBLICATIONS **0** CITATIONS

THE JOURNAL OF PHYSICAL CHEMISTRY B

Article

pubs.acs.org/JPCB

Spatial and Orientational Structure of the Hydration Shell of Benzene in Sub- and Supercritical Water

Ashu Choudhary and Amalendu Chandra*

Department of Chemistry, Indian Institute of Technology Kanpur, Kanpur, India 208016

Supporting Information

ABSTRACT: The spatial and orientational structure of the solvation shell of benzene in sub- and supercritical water are investigated by means of molecular dynamics simulations. The present study reveals different local organization of water molecules at different parts of the solute. The π-hydrogen-bonding between benzene and water along the axial direction is found to exist even at supercritical conditions although to a reduced extent. The coordination number of benzene decreases substantially on increase of temperature and decrease of density. While the π-hydrogen-bonded part in the axial region shows a slight expansion, the hydrophobically solvated part in the equatorial plane shows an opposite behavior as the temperature is increased from normal to the supercritical temperature. Two other distribution functions, namely the radial/angular and spatial orientational functions (SOFs) are calculated to explore the spatially resolved angular preferences of water molecules around the benzene solute. Water molecules located axial to the benzene are found to have strong inward orientation toward the solute, however an opposite behavior is found in the equatorial region. Although at supercritical conditions, the orientational distributions of water molecules are broadened, the preferential orientations in the axial and equatorial regions remain similar to that under ambient condition on average.

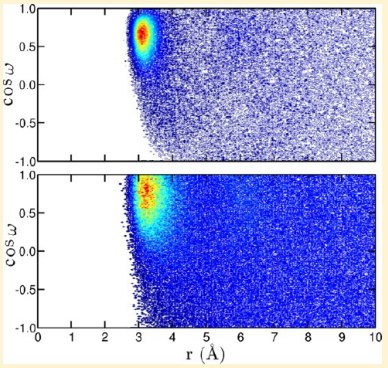

1. INTRODUCTION

Hydrophobic interaction between nonpolar molecules and water plays a significant role in many important chemical and biological processes including protein folding, molecular recognition and micelle formation.[1−11] The hydrophobic effect is associated with specific structural changes of water molecules surrounding a hydrophobe.[12−15] The water molecules adjust to the solute presence by changing the orientation and hydrogen bonding pattern in its vicinity. In case of aromatic solutes, the solute-water interaction is unique due to the attractive nature of the weak hydrogen bonding between π-electron cloud of aromatic rings and water hydrogens and the hydrophobic interaction between CH groups and oxygens of surrounding water molecules.[16,17] The π-hydrogen-bonding (πHB) is recognized as a common force at biological interfaces comprising of aromatic groups. In order to understand the nature of aromatic solute−water interactions, the simple aromatic hydrophobe of benzene molecule has been used as a prototype in many theoretical and vibrational spectroscopic studies in recent years.[16−26] There are other spectroscopic studies also available in the literature which investigated benzene aqueous solutions at ambient conditions and also at high temperatures and pressures[27−30] and suggested that the πH-bonding exists at ambient as well as at high temperatures. Recently, the existence of πH-bond between benzene and liquid water has also been studied by using Raman multivariate spectroscopy[31] which reported that approximately one πH-bond is formed between a dissolved benzene and surrounding water molecules located along the axial direction with respect to the plane of the benzene ring.

Supercritical aqueous solutions are widely used as important industrial solvents. Since aromatic hydrocarbons are prime candidates for hazardous waste destruction in supercritical water, studies of benzene−water interactions at supercritical conditions are therefore very important to understand such reactions. The temperature and density dependence of the hydration structure around a hydrophobic solute is useful to examine the hydrophobic solvation behavior in supercritical water. Experiments are difficult to perform at supercritical conditions. Also, experimental measurements of such properties give averages over all water molecules present in the hydration layer. Molecular simulations can provide information on spatially and orientationally resolved hydration shell with full microscopic details at atomic level.

The solvation structure of a benzene solute in aqueous solution has been studied earlier through molecular dynamics,[32−38] *ab initio* molecular dynamics[38−40] and Monte Carlo[41−45] simulations. In some of the earlier work,[36−41] specific attention was given to the distinct hydration pattern found in the axial and equatorial regions around benzene at ambient condition. However, only few studies have paid attention to the orientational aspects[36,39,40] which seem to be the key factor for such asymmetric solvation shells. In recent

Received: April 8, 2015
Revised: June 7, 2015
Published: June 25, 2015

DOI: 10.1021/acs.jpcb.5b03371
J. Phys. Chem. B 2015, 119, 8600−8612

years, the angular and spatially resolved solvation structure in sub- and supercritical water have also been studied for other aromatic solutes such as phenol, aniline, and naphthalene[46−48] by means of molecular dynamics simulations. In these work, simulations were performed for a phenol, aniline, or naphthalene solute dissolved in water at several temperatures along the liquid−vapor coexistence curve of water up to the critical point and also above the critical point with a fixed density of water. Spatial maps of local atomic solvent density around an aromatic solute were presented which provided a detailed picture of the solvent organization in the hydration shells including a quantitative analysis of the solute−water π-hydrogen-bonds for varying thermodynamic state points.[46−48] In the current work, we focus specifically on the spatial structure and orientation of water in the anisotropic solvation shell around benzene. Two specific distribution functions, namely the radial/angular distribution functions and spatial orientational functions (SOFs) are calculated, in addition to the radial distribution functions (RDFs) and spatial distribution functions (SDFs) of different axial and equatorial regions around the solute, to explore the changes in spatially resolved angular preferences of water molecules around the benzene solute as one moves from ambient to supercritical conditions.

The present study involves classical potentials for modeling water−water and benzene−water interactions.[36−38] We have carried out a series of molecular dynamics simulations to investigate the spatially and orientationally resolved hydration structure around benzene for varying temperature and solvent density. Specifically, we have studied a single benzene molecule dissolved in ambient water of density 1.0 g cm^{-3} at 298 K, in subcritical water of density 0.87 g cm^{-3} at 473 K and in supercritical water of two different solvent densities of 0.7 and 0.35 g cm^{-3} at 673 K. We note that the first two systems belong to the liquid side of water-vapor coexistence temperature curve and the density of 0.35 g cm^{-3} at 673 K is slightly above the critical density of water. Additionally, we have also simulated a fifth system of a benzene solute dissolved in supercritical water of density 1.0 g cm^{-3} at 673 K. This will allow us to compare the results of the ambient system with those at the supercritical temperature when one moves along the temperature axis following the constant density isochore of 1.0 g cm^{-3}. We note that although this system of 1.0 g cm^{-3} density at 673 K will have very high pressure and is unlikely to be prepared in an experimental scenario at present, consideration of such a system in a theoretical study has the advantage of providing information that otherwise is difficult to find through experiments. It may be noted that such a high density supercritical aqueous system was also considered in many earlier simulation studies of solvation in supercritical water.[49−58] The solvation structure of benzene in these solutions is studied through benzene−water pair correlations, radial/angular distribution functions, spatial distribution functions and also spatial orientation functions. Our study gives a detailed picture of the local organization at molecular level in terms of positional and orientational preference of water molecules around benzene at supercritical conditions and the variation of these structures from that at the ambient and subcritical conditions. Importantly, a contrasting structural behavior is found for the πH-bonded and hydrophobically solvated parts of the solvation shell of the solute on increase of temperature. While the πH-bonded part along the axial direction shows a little expansion, the hydrophobically solvated part in the equatorial plane undergoes a slight contraction similar to that found for a purely hydrophobic solute like methane as the temperature is increased from 298 K to the supercritical temperature of 673 K.

The organization of the rest of the paper is as follows. In section 2, we have described the models of water and benzene molecules that are employed here and also other details of the simulations. In section 3, the results of the angular and spatially resolved solvation structure of benzene are discussed. Finally, our conclusions are briefly summarized in section 4.

2. MODEL AND SIMULATION DETAILS

In the present work, the benzene and water molecules are characterized by multisite interaction models. In these models, the effective interaction between atomic sites i and j of two molecules is expressed as

$$u(r_i, r_j) = 4\epsilon_{ij}\left[\left(\frac{\sigma_{ij}}{r_{ij}}\right)^{12} - \left(\frac{\sigma_{ij}}{r_{ij}}\right)^{6}\right] + \frac{q_i q_j}{r_{ij}} \quad (1)$$

where, q_i and q_j are the charges of the ith and jth sites of interaction. The Lennard-Jones (LJ) parameters σ_{ij} and ϵ_{ij} are obtained by using the combination rules $\sigma_{ij} = (\sigma_i + \sigma_j)/2$ and $\epsilon_{ij} = (\epsilon_i\epsilon_j)^{1/2}$, where σ_i and ϵ_i are the LJ diameter and well depth parameter for the ith atom.

For benzene, we have employed the OPLS-AA (optimized potential for liquid simulations-all atom) 12-site model.[59] This model has 12 interaction sites with all the sites acting both as Lennard-Jones and charge interaction centers. The water molecules are characterized by the well-known SPC/E (simple point charge/extended) potential.[60] The values of the Lennard-Jones (LJ) and electrostatic interaction potential parameters for benzene and water are given in Table 1.

Table 1. Values of Lennard-Jones and Electrostatic Potential Parameters[a]

atoms	σ (Å)	ϵ (kJ/mol)	charge (e)
	Benzene		
C (r_{CC} = 1.4 Å)	3.55	0.2929	−0.115
H (r_{CH} = 1.08 Å)	2.42	0.1255	+0.115
	Water		
O	3.169	0.6502	−0.8476
H	–	–	+0.4238

[a] e represents the magnitude of electronic charge.

The current molecular dynamics simulations were conducted in a cubic box containing a single benzene molecule dissolved in 511 water molecules. Periodic boundary conditions with minimum image convention were employed in all three directions. The simulations were performed at 298 K for the solvent density of 1.0 g cm^{-3}, 473 K for the solvent density of 0.87 g cm^{-3} and at 673 K for the solvent densities of 0.70 and 0.35 g cm^{-3}. We will refer to these four systems as systems 1−4, respectively. Apart from these four systems, we also performed another simulation at 673 K for the solvent density of 1.0 g cm^{-3} which will be referred to as system 5. We note that systems 1 and 5 have the same density but at two very different temperatures, thus the results of these two systems can be compared to understand the effects of temperature on solvation structure at constant density although experimental realization of the latter system would be difficult due to its very high pressure. Nevertheless, we have made such comparisons of the

DOI: 10.1021/acs.jpcb.5b03371
J. Phys. Chem. B 2015, 119, 8600−8612

results of systems 1 and 5 which are presented in the Supporting Information.[61] We employed a spherical truncation of the Lennard-Jones interaction potential at 0.5L, where L is the edge length of the simulation box. The long-range electrostatic interactions were treated using the Ewald method.[62]

The size of the simulation box for a given system is determined by the density of water at that particular system. We employed the quaternion formulation of the equations of rotational motion and, for the integration over time, we adapted the leapfrog algorithm with a time-step of 1 fs. The initial velocities of all the molecules of a given system were taken from a Maxwell−Boltzmann distribution corresponding to the desired simulation temperature. For each system, we first ran the simulation for 5 ns for equilibration during which the temperature was kept fixed through velocity rescaling. After equilibration, each system was further run for a production phase of 10 ns. During the production run, velocity rescaling was employed only occasionally to prevent any significant drift from the desired temperature. This ensures that the average kinetic energy remains close to that corresponding to the desired macroscopic temperature for a given system. We used this production phase of the simulations to calculate various structural properties of the systems. We note that similar simulation protocols were also used in many of our earlier studies in recent years and also by others.[58,63−74] The average temperature and the associated fluctuations during the production phase are given in Table S1 of the Supporting Information.[61] Apart from the benzene-water systems, we also carried out five additional simulations of a single methane molecule in water for the same solvent densities and temperatures as in systems 1−5 for benzene in water. For methane, we used the OPLS potential model[59,75] and, for water, we used the same SPC/E model[60] that was used for benzene−water simulations. The lengths of the boxes and other simulation protocols remain the same as those of the benzene−water systems.

3. RESULTS AND DISCUSSION

The spatially and angularly resolved solvation structure of benzene is studied by considering different conical regions around the benzene solute. These regions are defined as (a) axial region which is defined as the region orthogonal to the ring plane. The angle θ_{axial} of the axial cone is defined as the angle between the principal axis of C_6 symmetry of the solute and a vector along the surface of the cone. (b) Second is the equatorial region which is defined as the region in the ring plane. The angle θ_{equa} of equatorial cones is defined as the angle between any of in-plane C_2 axis using benzene center as the reference point and a vector along the surface of the cone (Figure 1). The volume of the axial region with conical angle θ_{axial} is given by

$$V_{\theta}^{axial} = (4\pi/3)(1 - \cos\theta_{axial})r^3 \quad (2)$$

and the volume of the equatorial region with the conical angle θ_{equa} is

$$V_{\theta}^{equa} = (4\pi/3)(\cos(90 - \theta_{equa}))r^3 \quad (3)$$

where r is the slant height of the cones.

3.1. Radial Distribution Functions for Axial and Equatorial Regions. The radial distribution functions (RDFs) provide useful information about the orientally arranged local environment around a particular species. For a symmetrically solvated solute, the RDFs can be calculated by considering the spherical shells and then normalizing those by the uniform bulk density.[62] However, for solute molecules like benzene which has anisotropic solvation shell, this approach does not provide information about anisotropic interaction between the benzene and water molecules. In order to capture the anisotropic nature of the solvation shell, we have divided the solvation shell into equatorial and axial regions by taking the benzene center of mass, denoted as Bz, as the reference point and then calculated benzene−oxygen ($g_{Bz-O}(r)$) and benzene-hydrogen ($g_{Bz-H}(r)$) RDFs separately for the axial and equatorial regions[36−41] for different values of the corresponding conical angles.

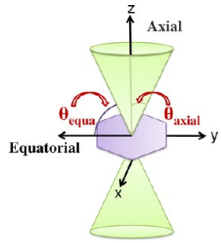

Figure 1. Axial and equatorial regions around a benzene molecule. The angle of axial cone (θ_{axial}) is the angle with the principal axis of C_6 symmetry and the angle of the equatorial cone (θ_{equa}) is the angle with any of the C_2 axis of symmetry of the benzene molecule.

The Bz−O and Bz−H RDFs for the first four systems in the axial regions characterized by conical angles of 20°, 45°, 60°, and 90° are shown in Figure 2. It is found that, for the axial conical region of 20°, all Bz−O RDFs have a single peak at around 3.1−3.2 Å. The height of this peak is relatively large for system 1 compared to other systems as can be seen from Figure 2a. For Bz−H RDFs, Figure 2e shows that the axial conical region of 20° has two peaks for systems 1−2 at around 2.3 and 3.5 Å, while these two peaks appear to be diminished for the supercritical systems 3−4. The Bz−O peak at 3.1 Å and the Bz−H peak at 2.3 Å for system 1 correspond to πH-bonded configurations.[36−41] With increase of angle of the axial conical region, the positions of these peaks for system 1 remain unchanged, however the peak heights gradually decrease which is likely because this weak structural feature is averaged out by other molecules when larger axial regions are considered.

For systems 2−4, the prominent peaks in the π H-bonding region of Bz−O and Bz−H correlations essentially disappear for higher values of the axial conical angle. A small shoulder is found at distance up to 2.9 Å for the Bz−H RDFs in the 45° axial region of RDFs for systems 2−4 (Figure 2f). This shows the existence of πH-bonding interaction between benzene and water, although to a lesser extent, even at supercritical conditions. This small shoulder almost disappears in the 60° and 90° axial regions which is again likely because this weak effect is averaged out by other molecules when the larger axial regions are considered (Figure 2g,h). This implies that the πH-bonding is a specific feature for the small axial conical regions and this interaction exists to some extent even at higher temperatures of sub- and supercritical conditions. The Bz−O and Bz−H RDFs for the axial regions of 45°, 60°, and 90° cones have two peaks for system 1, while only a single prominent broad peak is observed for systems 3 and 4. For system 2, a shoulder followed by a broad peak are found. The second peak for system 1 evolves with increase in the angle of

DOI: 10.1021/acs.jpcb.5b03371
J. Phys. Chem. B 2015, 119, 8600−8612

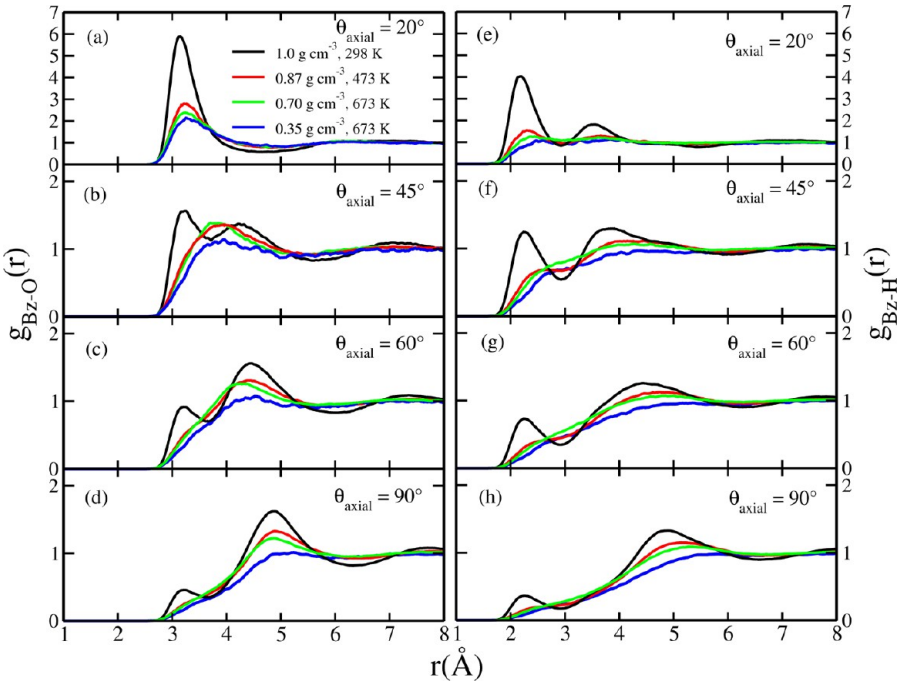

Figure 2. Radial distribution functions (RDFs) between the center of mass of benzene (Bz) and oxygen atoms of water are plotted in parts a–d for 20°, 45°, 60°, and 90° axial conical regions of the benzene solvation shell, respectively. The corresponding plots for Bz–H RDFs are shown in parts e–h.

the axial conical regions with its peak position around 4.8 Å for the 90° axial conical region. This peak at 4.8 Å for θ = 90° represents the total solvation shell for system 1 (see Figure 2d). Systems 2–4 also have a peak maximum above 4.5 Å for the 90° axial conical region corresponding to the formation of a solvation shell. All the peaks of Bz–H and Bz–O RDFs for systems 2–4 are broader because the thermal effects at the supercritical temperature tend to randomize the positions of molecules due to higher translational and rotational kinetic energy. The observed changes in the RDFs with change of temperature from ambient to subcritical to supercritical conditions and also with the decrease of densities at the supercritical temperature reveal that the structure of water around benzene is less ordered under supercritical conditions. Also, a critical analysis of the RDFs for the 20° and 45° axial regions reveal an expansion of the πH-bonded part of the solvation shell on increase of temperature. For example, the locations of the first maximum and minimum of the Bz–O RDF for the 20° axial region increases from 3.12 and 4.65 Å to 3.25 and 4.74 Å, respectively, as the temperature is increased from 298 (density 1.0 g cm^{-3}) to 673 K (density 0.35 g cm^{-3}). The other systems at the supercritical temperature show similar expansion of the πH-bonded part as can be seen from the data presented in Table 2. A comparison of the RDFs for systems 1 and 5 are shown in Figure S1 of the Supporting Information.[61] These results again show a decrease in the peak heights of both Bz–O and Bz–H correlations even when the density is kept constant while increasing the temperature from 298 to 673 K. Other characteristics of the RDFs of system 5 such as the locations of the first maximum and minimum are included in Table 2 for the 20^o axial region.

The Bz–O and Bz–H RDFs for the equatorial regions with angles (θ_{equa}) of 20°, 45°, 60°, and 90° are shown in Figure 3 for systems 1–4. The Bz–O and Bz–H RDFs for the 20°, 45°, and 60° equatorial regions are found to have only a single peak

Table 2. Locations of the First Maximum (r_{max}) and Minimum (r_{min}) of Benzene–Water Bz–O RDFs in the 20° Axial and 20° Equatorial Regions of the Benzene Solvation shell for Systems 1–5, Where Bz Stands for the Center of Mass of Benzene and Systems 1–5 Are Defined in Section 2

conical region	system 1	system 2	system 3	system 4	system 5
			20° Axial		
r_{max}	3.12	3.21	3.20	3.25	3.19
r_{min}	4.65	4.65	4.74	4.74	4.70
			20° Equatorial		
r_{max}	4.98	4.95	4.90	4.96	4.75
r_{min}	6.68	6.66	6.36	6.38	6.32

for all the systems. In Figure 3, the Bz–O and Bz–H RDFs for the smaller equatorial regions of systems 2–4 appear little closer to the benzene in the equatorial regions which is likely due to the influence of thermal effects. The Bz–O and Bz–H RDFs for the larger equatorial regions reveal a secondary peak at around 3.2 and 2.3 Å, respectively, before the main peak at ~4.8 Å which shows that the water molecules come closer to the benzene as the angle of the equatorial region increases due to contributions from the πH-bonded water molecules. It is to be noted that 90° axial and 90° equatorial regions represent the total solvation region around benzene. So, the RDFs of the 90° equatorial region are found to be identical to the 90° axial and show evidence of πH-bonding. With increase in temperature and decrease in density, the peak heights of the 90° equatorial region are found to decrease which can be attributed to an overall weakening of the solvation shell around the benzene with increase of kinetic energy and decrease of density. The equatorial regions of smaller conical angles, e.g., 20° or 45°, capture only the hydrophobically solvated water molecules without any contributions from πH-bonded molecules. The location of the first peak of the Bz–O RDFs of the 20° or 45°

DOI: 10.1021/acs.jpcb.5b03371
J. Phys. Chem. B 2015, 119, 8600–8612

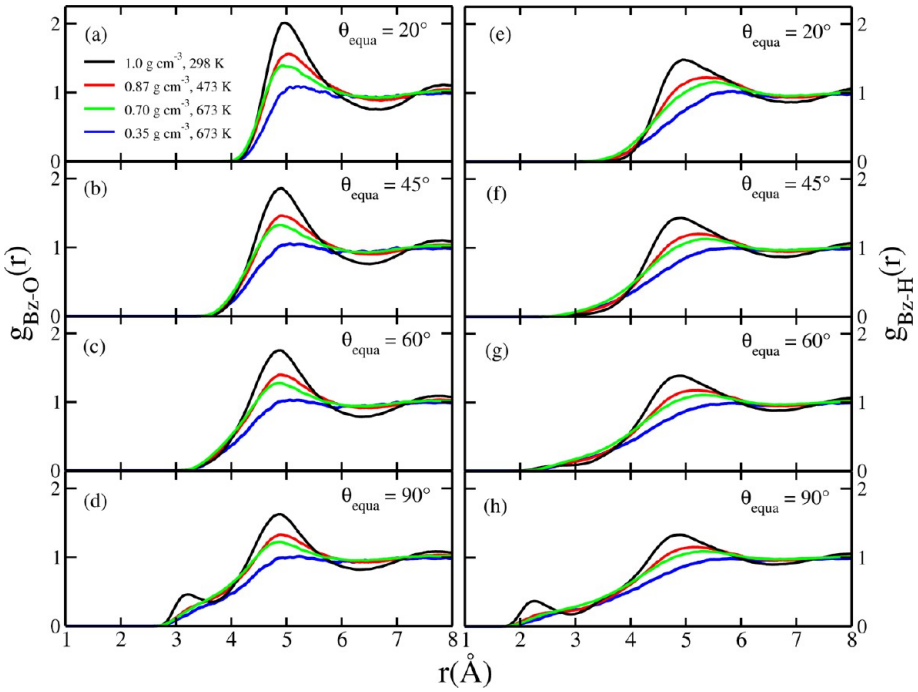

Figure 3. Benzene center of mass (Bz)−oxygen RDFs are plotted in parts a−d and Bz−H RDFs are plotted in parts e−h for 20°, 45°, 60°, and 90° equatorial conical regions of the benzene solvation shell, respectively.

equatorial regions clearly reveal a contraction of the hydrophobically solvated part of the solvation shell on increase of temperature. The locations of the first maximum of the main peak of Bz−O RDF at around 5 Å and the minimum that follows the maximum for 20° equatorial regions of all the systems are included in Table 2. A comparison of the corresponding RDFs for systems 1 and 5 are shown in Figure S2 of the Supporting Information,[61] which again shows a slight contraction of the hydrophobically solvated part of the benzene solvation shell. In order to verify the generality of this behavior, we carried out additional simulations of a purely hydrophobic methane solute in normal and supercritical water. The C−O RDFs of these methane-water systems are shown in Figure.S3 and the locations of the first maximum and minimum of the C−O RDFs are included in Table 3. The results of Figure S3

Table 3. Locations of the First Maximum (r_{max}) and Minimum (r_{min}) of Methane−Water C−O RDFs for Systems 1−5[a]

solvation shell	system 1	system 2	system 3	system 4	system 5
r_{max}	3.74	3.70	3.68	3.72	3.52
r_{min}	5.41	5.40	5.28	5.30	5.10

[a]Note that systems 1−5 correspond to those described in section 2 except that the benzene solute is replaced by a methane solute.

and Table 3 also show a contraction of the solvation shell of methane on increase of temperature. Thus, the contraction of the hydrophobically solvated part of the hydration shell of benzene on increase of temperature can be regarded as a general behavior of the hydration shell of hydrophobic solutes. We note that the RDFs of the axial and equatorial regions represent the orientationally averaged water structure around benzene. By definition, RDFs do not capture the details of orientational structure of water molecules.

We have also calculated the π H-bond number and also the coordination number of the benzene solute by integrating the Bz−H and Bz−O RDFs up to appropriate cutoff distances. Integration of the Bz−H radial distribution function up to 2.9 Å determined the average number of πH-bonds[31,38] which are included in Table 4 for systems 1−5. It is seen that at ambient

Table 4. π-H Bond and Coordination Numbers of Benzene for Systems 1−5

quantity	system 1	system 2	system 3	system 4	system 5
number of πH bonds	1.20	0.81	0.53	0.18	1.07
coordination number	31.26	26.29	20.04	8.43	30.33

condition, benzene forms on average 1.2 πH-bonds with water which is in good agreement with the value of 1.3 reported earlier for a different model of water.[38] The number of πH-bonds decreases to 0.81, 0.53, and 0.18 for systems 2−4, respectively. This shows that πH-bonding is greatly reduced by increase of temperature and decrease of density. The trends of these results are in general agreement with the findings of previous studies of other aromatic solutes in sub- and supercritical water.[46−48] For example, the number of πH-bonds for phenol (aniline) were found to be 0.84 (0.75) and 0.46 (0.47) for water densities of 1.0 g cm^{-3} (298 K) and 0.87 g cm^{-3} (473 K), respectively, in the work of ref.[46,47] For naphthalene and benzene, the πH-bond numbers were found to be 1.17 and 1.14, respectively, for ambient water.[48] The oxygen atom coordination numbers of benzene, which are obtained by integrating the Bz−O correlations up to 6.3 Å, i.e., over the first solvation shell, are also included in Table 4 for all the systems. It is seen that the average number of water molecules in the solvation shell decreases from 31 for system 1 to 26, 20, and 8 for systems 2−4, respectively, on increasing the temperature and decreasing the density. Thus, the solvation shell for the

DOI: 10.1021/acs.jpcb.5b03371
J. Phys. Chem. B 2015, 119, 8600−8612

higher temperature and lower density systems is rather thinly populated unlike a dense solvation shell formed at the ambient condition. In order to capture the orientational aspects of water around benzene under supercritical conditions, we next discuss the radial/angular distribution functions which represent structural probability functions resolved in both radial and tilt angle coordinates.

3.2. Radial/Angular Distribution Functions. In order to gain information about the relative orientation of water molecules around the benzene solute, we have calculated the radial/angular distribution functions of the dipole moment ($g_{Bz-O}(r, \cos\omega)$) and O−H bond ($g_{Bz-O}(r, \cos\alpha)$) vectors of water molecules present around benzene.[36] The tilt angles ω and α are defined in Figure 4. We note that ω is the angle between the radial vector $\vec{r}$ and water dipole vector $\vec{\mu}$ as shown in Figure 4a and α is the angle between the radial vector $\vec{r}$ and O-H bond vector of water as shown in Figure 4b, where $\vec{r}$ is the vector joining the benzene center of mass to the water oxygen and $\vec{\mu}$ is the unit vector originating from oxygen center and passes along the angle bisector of the HOH angle. These functions are two-dimensional distribution functions resolved in both distance and tilt angle coordinates. For the isotropic distribution in bulk, the values of probability densities are the same for different values of cos ω and cos α in the range of −1.0 to +1.0. The usual normalization is done in the radial dimension (r), therefore the value of the bulk density is around unity. The relative values of the density in different regions can be compared with the color-bar associated with each figure.

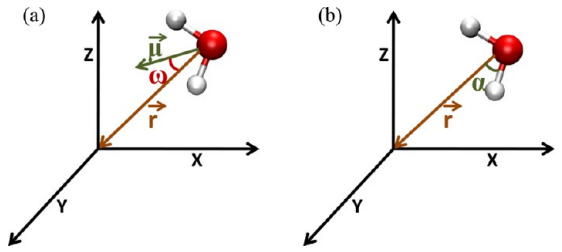

Figure 4. Definition of molecular vectors and tilt angles of a water molecule in the benzene solvation shell: The benzene center of mass is taken as the origin, the $\vec{r}$ is defined as the vector joining the benzene center of mass to the water oxygen and $\vec{\mu}$ is the unit vector along the HOH angle bisector originating from oxygen. (a) Tilt angle ω is the angle between $\vec{r}$ and dipole vector $\vec{\mu}$. (b) Tilt angle α is the angle between $\vec{r}$ and OH bond vector.

We have calculated the radial/angular distribution functions for water dipole ($g_{Bz-O}(r, \cos\omega)$) and O−H ($g_{Bz-O}(r, \cos\alpha)$) orientations for the axial and equatorial conical regions of 20°, 45°, 60°, and 90° angles in order to find the angular preference of water molecules in different parts of the benzene solvation shell. The angular bin width of 1.0° and distance bin width of 0.05 Å, were used in our calculations. These tilt angle resolved correlations for the axial and equatorial regions provide information about the changes in the orientation of water molecules because of anisotropic interactions with the benzene solute. The orientational preference of water around benzene can be clearly extracted from the radial/angular distribution functions in conjunction with Bz−O RDFs. The results of $g_{Bz-O}(r, \cos\omega)$ are shown in Figure 5 for systems 1−4 for the axial conical regions around benzene with θ_{axial} = 20°, 45°, 60°, and 90°. The corresponding results for system 5 are shown in Figure S4 of the Supporting Information.[61] In Figure 5, Systems 1−4 are arranged from left to right in the figure, with their increased conical angle from top to bottom. The results of $g_{Bz-O}(r, \cos\omega)$ for the axial conical region of θ_{axial} = 20° are shown in Figure 5a−d for systems 1−4, respectively. It is found that for systems 1−4, there is a well-defined maximum at

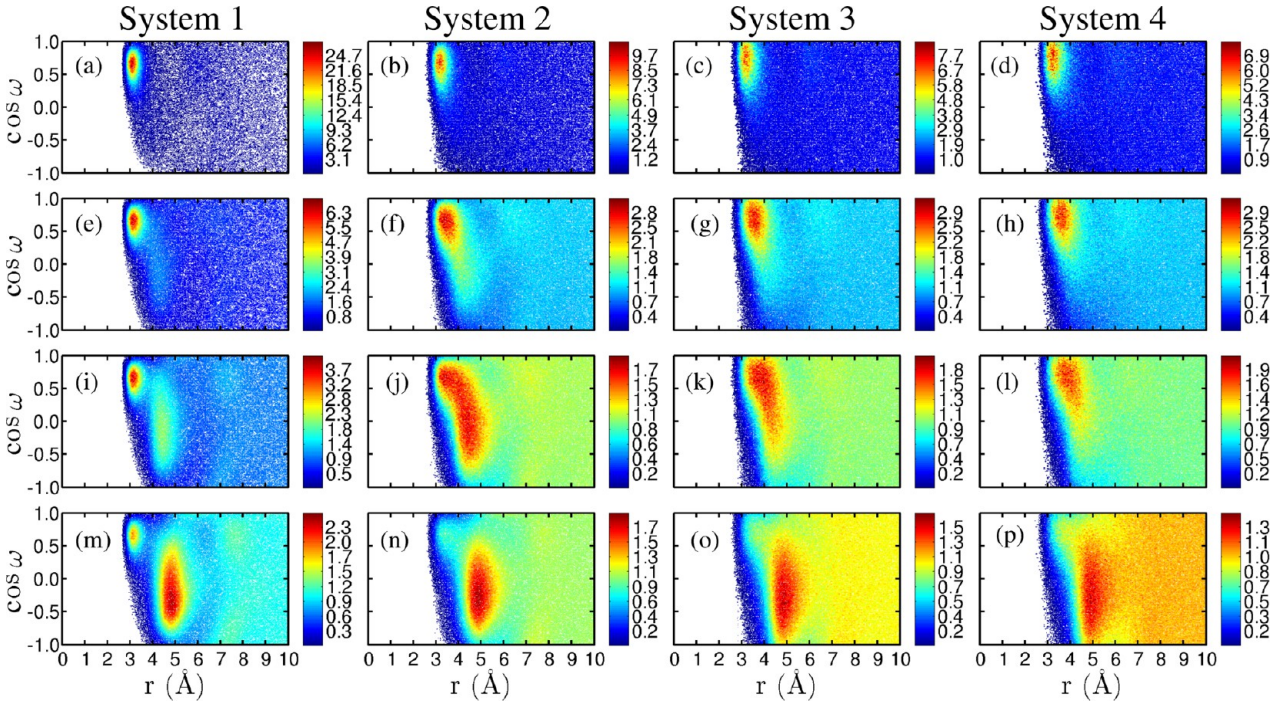

Figure 5. Radial/angular distribution functions of water position and dipole tilt angle, $g_{Bz-O}(r,\cos\omega)$, in the axial region of the solvation shell of benzene are arranged from left to right for systems 1−4, respectively. For each system, the top to bottom figures are for the axial conical regions of θ_{axial} = 20°, 45°, 60°, and 90°, respectively.

DOI: 10.1021/acs.jpcb.5b03371
J. Phys. Chem. B 2015, 119, 8600−8612

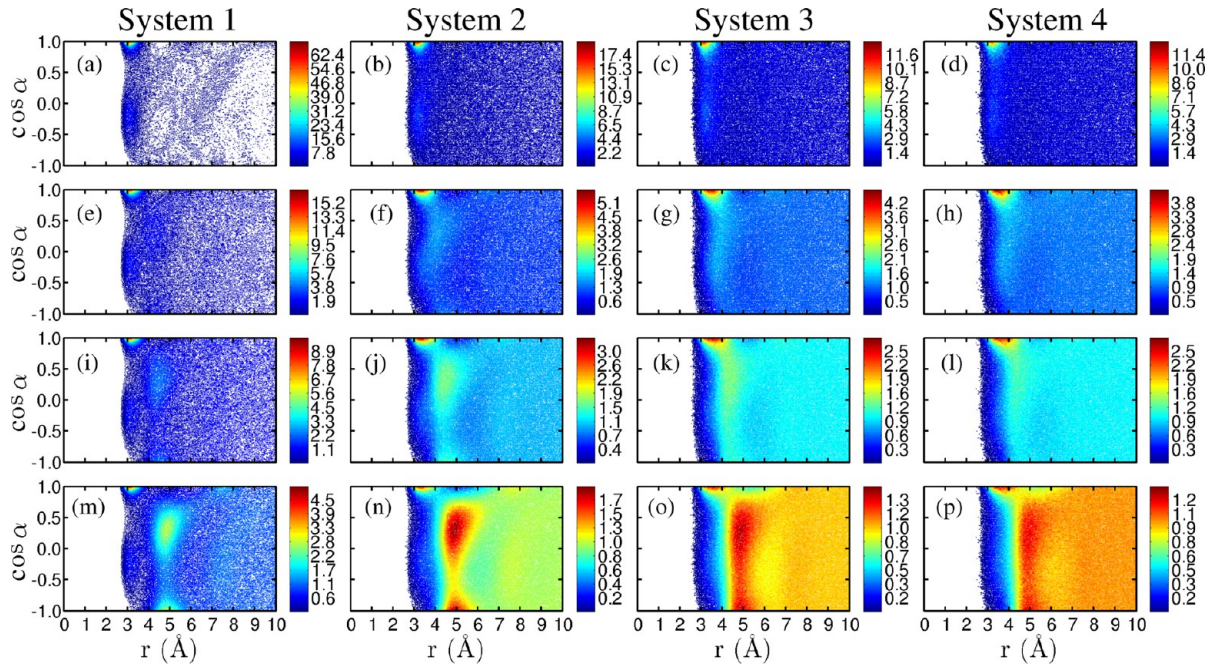

Figure 6. Radial/angular distribution functions of water position and OH tilt angle, $g_{Bz-O}(r, \cos \alpha)$, in the axial region of the solvation shell of benzene are arranged from left to right for systems 1−4, respectively. For each system, the top to bottom figures are for the axial conical regions of θ_{axial} = 20°, 45°, 60°, and 90°, respectively.

around 3.1−3.2 Å, for cos ω = 0.63, *i.e.*, ω = 51°. The peak heights in associated color bars show that the relative probability density in the 20° axial region is relatively higher than that in the corresponding larger axial regions for a particular system. This means that the maximum probability for water molecules in the axial region is to align one of their O−H vector toward $\vec{r}$. Similar conclusion can also be made from the results of system 5 shown in Figure.S4. Thus, the water molecules in the axial regions at the higher temperatures of sub- and supercritical conditions also tend to keep a preferential alignment similar to that at the ambient condition although to a reduced extent.

For system 1, the $g_{Bz-O}(r, \cos \omega)$ shows two distinct peaks in the larger axial conical regions as it was found in the RDFs. Interestingly, both peaks have separate ranges of tilt angles. For systems 2−4, however no such distinct peaks appear but a wider range of tilt angles are found to be populated below cos ω = 0.5. The water molecules of systems 2−4 prefer to be within the small axial regions as shown by the relative density and angular preference in the 45° and 60° axial conical regions (Figure 5parts f−h and parts j−l). This fact suggests that the axial interaction holds the molecules more effectively even at lower density at the supercritical temperature. This observation would be more clear in the spatial distribution functions discussed later. For systems 2−4, the corresponding peaks are diffused relative to system 1 because greater thermal effects induce more rotational freedom to water molecules. The relative intensity of the peaks is also found to be low. Similar features are found for all the axial as well as equatorial radial/angular distribution functions for systems 2−4.

It is clear from Figure 5 that water molecules in the smaller axial regions have small tilt angle which is characteristic of π H-bonding. As we go from smaller to larger axial regions, the peak above 4.0 Å, evolves and the corresponding tilt angles show that the water molecules are arranged with a wider range of the tilt angle ω around the benzene solute. For system 1, in the 90° axial region, a broad distribution of the tilt angle with its maximum in the range of cos ω = −0.2 to −0.5 is found. This corresponds to the value of ω from 100° to 120° which is a characteristic feature of hydrophobic solvation. The more prominent peak at around 4.8 Å, for the 90° axial region for all the systems also supports the fact that the C−H peripheral region of benzene is more hydrophobic (see Figure 5m−p). For systems 2−4, it is seen that the preferred orientation of water molecules in small axial regions is quite similar to that at the ambient condition, however diffused due to enhanced thermal effects. The sharp transition in peaks from 60° to 90° axial region suggest that the number of molecules in the 60−90° axial conical shell dominates the behavior of the curve for the 90° axial region. With decrease in density of water at supercritical temperature, the smaller tilt angle regions are found to have relatively higher localized density compared to that in the corresponding bulk regions.

The contour plots in Figure 6 show the OH tilt angle resolved radial distribution functions ($g_{Bz-O}(r, \cos \alpha)$) for all the four systems in the axial conical regions of θ_{axial} = 20°, 45°, 60°, and 90° angles. In this figure, systems 1−4 are arranged from left to right and increased conical regions are arranged from top to bottom. The results of ($g_{Bz-O}(r, \cos \alpha)$) for the axial regions of system 5 are shown in Figure.S4. For system 1, the 20° axial conical region is found to have a maximum probability at around 3.1 Å and the OH vectors are found to maintain two distinct peaks around cos α values of 1.0 and −0.25 corresponding to α = 0° and 105°, respectively (Figure 6(a)). This shows that the water molecules in this region prefer to orient with one of their OH bonds pointing toward $\vec{r}$ and the second OH pointing away from $\vec{r}$. This is also expected from the dipole orientation picture discussed above for the same region. Similar orientational structure is found for the supercritical systems although with lower relative intensities as can be seen from Figures.6(b)-(d).

DOI: 10.1021/acs.jpcb.5b03371
J. Phys. Chem. B 2015, 119, 8600−8612

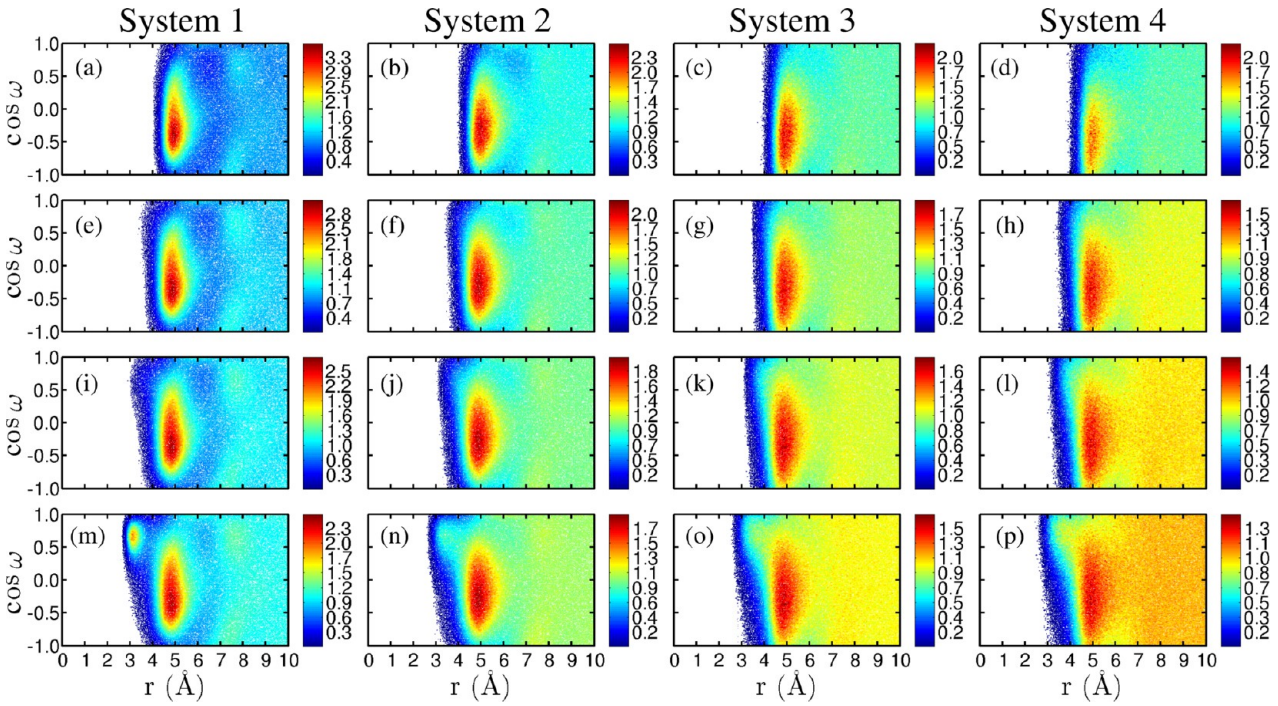

Figure 7. Radial/angular distribution functions of water position and dipole tilt angle, $g_{Bz-O}(r, \cos \omega)$, in the equatorial region of the solvation shell of benzene are arranged from left to right for systems 1−4, respectively. For each system, the top to bottom figures are for the equatorial conical regions of θ_{equa} = 20°, 45°, 60°, and 90°, respectively.

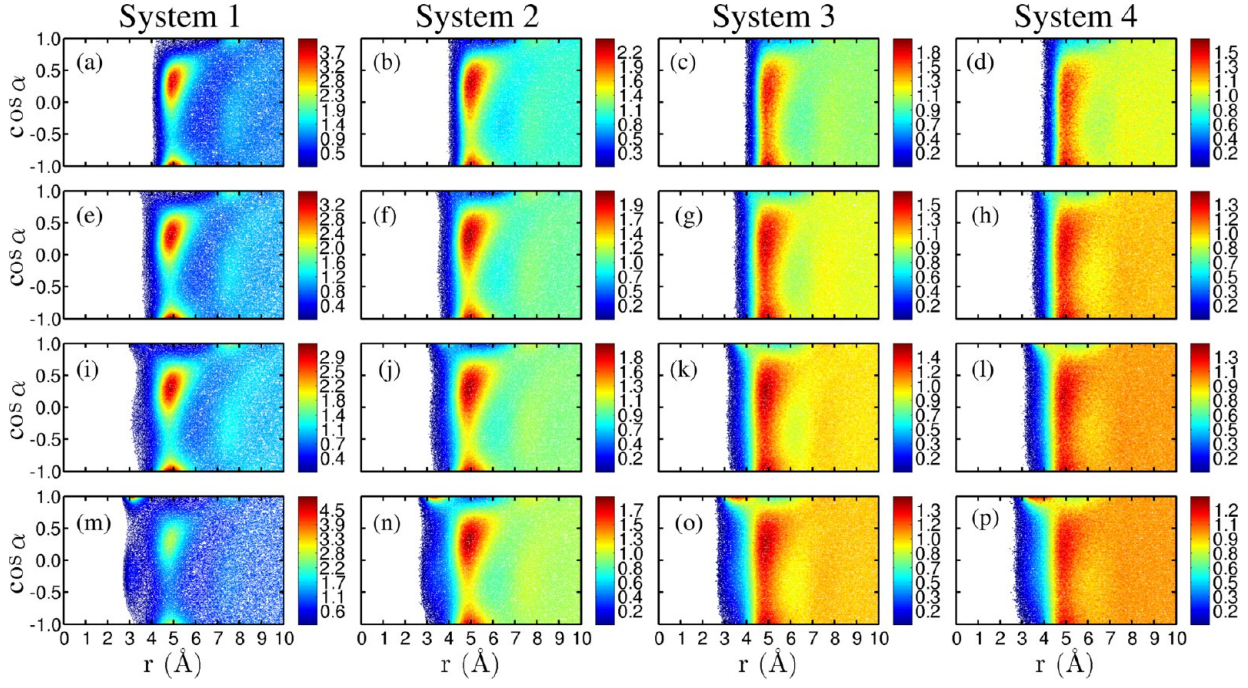

Figure 8. Radial/angular distribution functions of water position and OH tilt angle, $g_{Bz-O}(r, \cos \alpha)$, in the equatorial region of the solvation shell of benzene are arranged from left to right for systems 1−4. respectively. For each system, the top to bottom figures are for the equatorial conical regions of θ_{equa} = 20°, 45°, 60°, and 90°, respectively.

In the larger axial regions, additional peak is found to evolve at distances above 4.0 Å. Interestingly, the peak above 4.0 Å, has its maximum at around cos α = 0.3 and −1.0, corresponding to α = 73° and 180°, respectively. This configuration is almost opposite to what we observed for the smaller axial conical region of θ_{axial} = 20°. This shows that for the second peak, the most preferred orientation of water OH vectors is the one where one OH vector lies approximately tangential to the $\vec{r}$ and the other points opposite to the $\vec{r}$. Although thermal effects tend to randomize the orientation of water molecules at higher temperatures of sub- and supercritical conditions, still a preference for similar OH bond tilt angle is found to persist to a large extent. This is an indication of the presence of πH-bonding orientation of water OH vectors even

DOI: 10.1021/acs.jpcb.5b03371
J. Phys. Chem. B 2015, 119, 8600−8612

at supercritical temperature. Because of the thermal effects at higher temperature, a range of orientations for OH vectors is found in the solvation shell of the benzene molecule. The maximum probability region shifts to larger distances and becomes broader for lower densities which means weakening of the solvation shell and also more random OH vector orientation in the solvation shell of benzene with decrease of density at supercritical temperature. This is clearly seen in Figure 6n−p.

Next, we discuss the changes of dipole orientation of water molecules in the equatorial regions for increasing values of the conical angle θ_{equa}. We have shown the radial/angular correlation functions $g_{Bz-O}(r, \cos \omega)$ and $g_{Bz-O}(r, \cos \alpha)$ for θ_{equa} = 20°, 45°, 60°, and 90° in Figures 7 and 8, respectively, for systems 1−4 and the corresponding results for system 5 are shown in Figure S5. It is found that for all the four systems, the distributions start after 4.0 Å in the 20° equatorial region similar to the corresponding angle averaged RDFs shown in Figure 3. At ambient condition, it has a wider maximum range of cos ω from −0.2 to −0.5 (Figure 7a). The corresponding broad maxima for cos α are found at around 0.3 and −1.0 for the small equatorial regions (Figure 8a). These values correspond to ω = 100−120° and α = 75° and 180°, which show the outward orientation of water dipoles from benzene in the equatorial region, with one OH almost tangential to benzene and other opposite to $\vec{r}$. It may be noted that the region corresponding to the peak at 3.2 Å also gets dense with increase in the volume of the equatorial conical region and the main changes can be seen from 60° to 90° equatorial regions similar to what was found for the angle averaged RDFs of Figure 3. A preference for smaller values of the dipole and OH tilt angles is seen in the 3.0−3.5 Å distance range for both ambient and supercritical systems, which again indicates the existence of πH-bonding even at supercritical temperature although with a decreased intensity. The peak above 4.0 Å has higher tilt angle ranges for the dipole and OH vectors which is an indication of the hydrophobic nature of benzene. Similar conclusions can also be arrived at from Figure S5, where results of the two same-density (1.0 g cm^{-3}) solutions at 298 K (system 1) and 673 K (system 5) are compared. The radial/angular distribution functions clearly depict the benzene-water interactions in hydrophobic and hydrophilic terms. One can clearly connect the angular preference of water dipole and OH vectors to the peaks observed in Bz−O and Bz−H RDFs.

3.3. Spatial Distribution Functions in Cartesian Space.

We have calculated the spatial distribution functions (SDF) of oxygen atoms in terms of Cartesian coordinates around benzene for all the four systems. These SDFs describe the three-dimensional (3D) distribution of water molecules surrounding the benzene solute and capture changes in the three-dimensional solvation shell on changes of temperature and density. The SDFs are calculated in the Cartesian space by monitoring the positions of oxygens in a body fixed frame of benzene using the method similar to that of refs 37, 46−48, 76, and 77. In the present calculations, the body fixed frame is taken to be centered at the benzene center of mass. All the SDFs were normalized relative to bulk water density obtained from a pure water simulation performed at ambient condition. Hence, the calculated oxygen densities in benzene−water systems provide information regarding the relative densities with respect to ambient pure water system.

The SDFs for systems 1−4 are shown in Figure 9. The top view is shown in Figure 9a−d and corresponding side view of all the SDFs is shown in Figure 9e−h. The SDF results of system 5, along with those of system 1 for the purpose of comparison, are shown in Figure S6 of the Supporting Information.[61] The top and side views of oxygen density are plotted with two isovalues of 1.2 and 2.2 in transparent yellow and blue colors, respectively. The two-color representation is used to visualize higher and lower density regions together and to observe the changes occur in these regions with temperature and density. It is found that the axial region around the C_6-axis i.e. πH-bonded region and the regions in between the hydrogens in the equatorial plane are populated with higher oxygen density. On decreasing the density, gradual weakening of the hydration shell occurs first in the equatorial region and then in the axial region. Hence, the axial region is preferred more by the hydration shell water molecules at supercritical temperature even at lower densities. The higher thermal energy of supercritical water leads to the differences in the SDFs for systems 1 and 5 since these two systems have the same density. This is clear from the more homogeneous solvation shell around benzene for the same density at supercritical temperature as can be seen from Figure.S6.

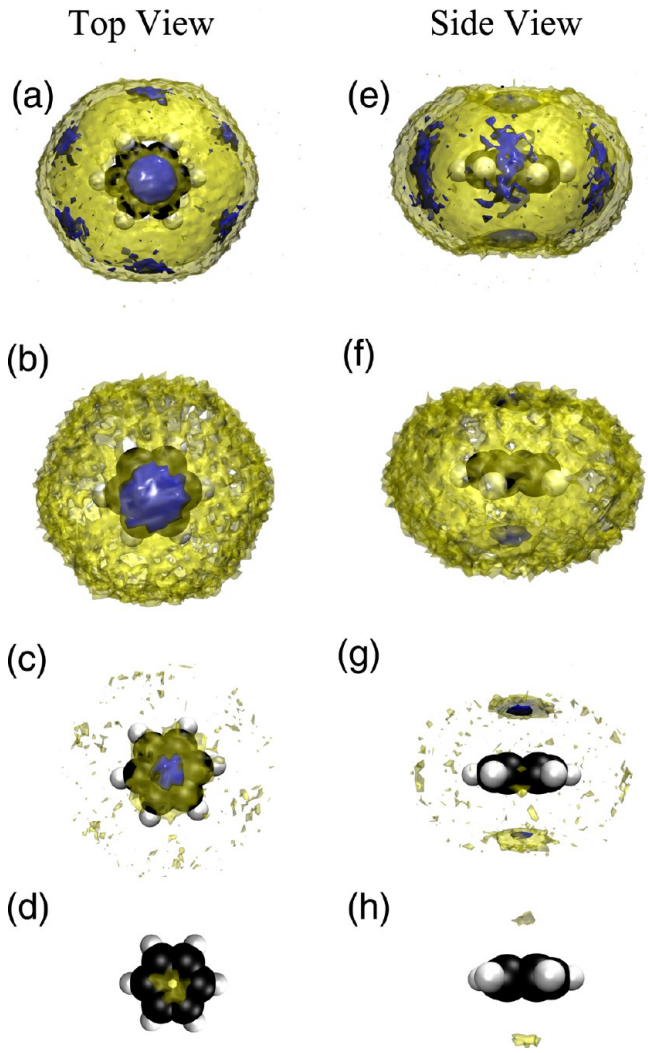

Figure 9. Spatial distribution functions in Cartesian space are plotted for systems 1−4. The top views are shown in parts a−d and the corresponding side views are shown in parts e−h. The surfaces of isovalue above 1.2 are plotted in transparent yellow and those with isovalue above 2.2 are plotted in blue color.

DOI: 10.1021/acs.jpcb.5b03371
J. Phys. Chem. B 2015, 119, 8600−8612

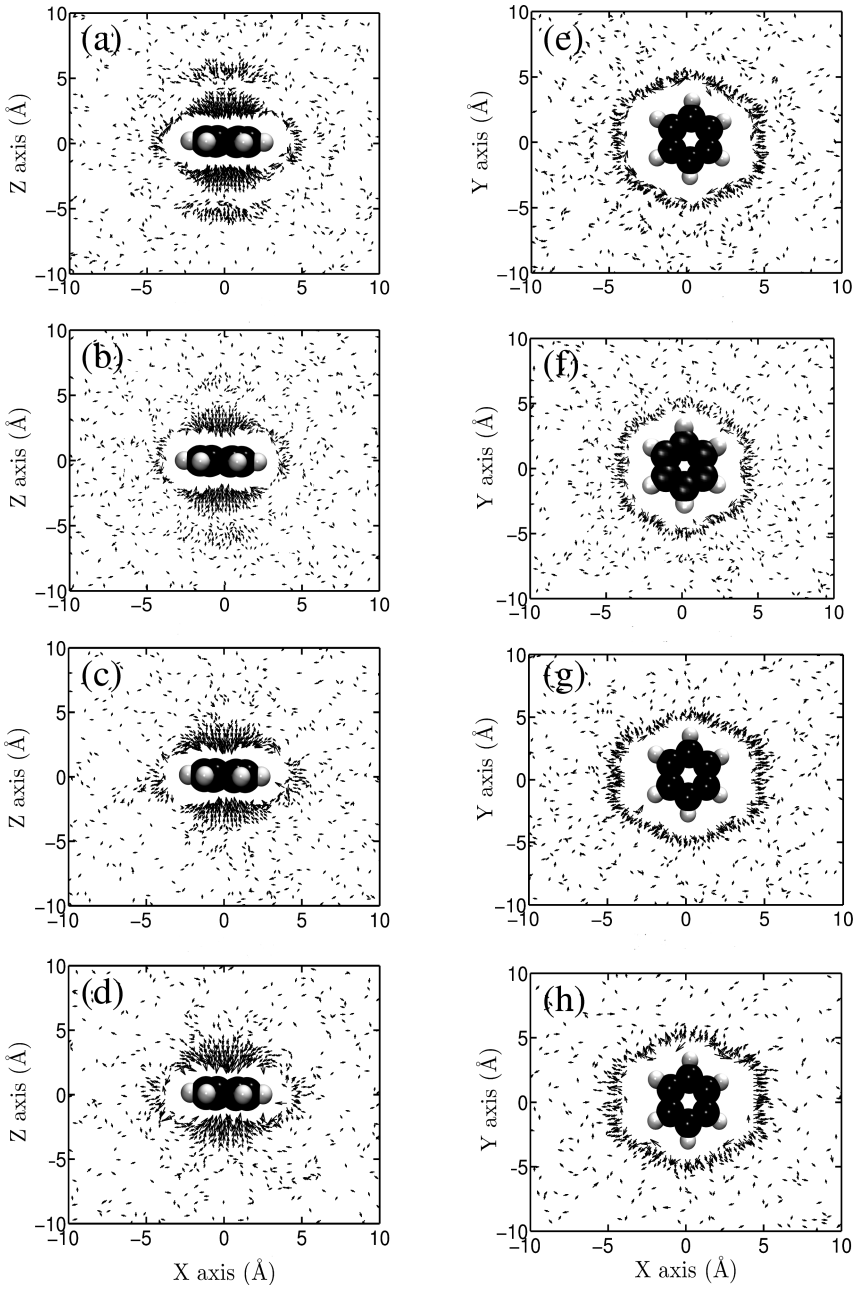

Figure 10. Spatial orientational functions of water molecules surrounding the benzene solute. Time averaged dipole $\langle \vec{\mu} \rangle$ projections for systems 1−4 along the *xz* slice are shown in parts a−d. The corresponding projections along the *xy* slice are shown in parts e−h.

The differences between the SDFs of system 1 and those of systems 2−4 seen in Figure 9 can be attributed to both temperature and density effects. Again, the presence of relatively higher oxygen density above and below the benzene plane around C_6-axis for the current systems reveals the existence of πH-bonding even at supercritical conditions. The absolute magnitude of the density around the benzene solute, however, is found to be greatly reduced as one moves to the sub- and supercritical water which is consistent with a highly reduced coordination number of benzene in the sub- and supercritical systems of lower densities compared to that of the ambient system (Table 4).

3.4. Spatial Orientational Functions. The spatial orientational functions (SOFs) measure the average orientation of water molecules in different parts of the three-dimensional (3D) space.[36] The orientation of a water molecule is described by its dipole vector $\vec{\mu}$. The individual components of $\vec{\mu}$ are considered with the positions of water oxygen similar to SDFs. Then, the sum of the individual *x*, *y*, and *z* components of $\vec{\mu}$ are stored for each 3D voxel and these individual component sums are then divided by the total oxygen count in the 3D position voxel. The resulting components give the average water orientation vector, $\langle \vec{\mu} \rangle$, within each voxel.[36] The number of voxels considered is fixed at 250 for all the systems.

We have calculated the SOFs of water around benzene in the form of slices cut through the three orthogonal planes of *xy*, *xz*, and *yz* with respect to the benzene C_6-axis (*z*-axis). The slices obtained through *yz* and *xz* planes are identical and demonstrate the axial region projections of the benzene solvation shell. The slices through *xy* plane show the projection

DOI: 10.1021/acs.jpcb.5b03371
J. Phys. Chem. B 2015, 119, 8600−8612

of the solvation shell in equatorial region. We have shown the *xy* and *xz* slices of SOFs for systems 1−4 in Figure 10. The corresponding results of system 5 are shown in Figure.S7 of the Supporting Information.[61] These slice plots in the *xy* and *xz* planes illustrate the projection of the averaged water orientation vector, $\langle\vec{\mu}\rangle$, on the respective planes. Each arrow tail originates from its voxel position and the arrow length is proportional to the projection of $\langle\vec{\mu}\rangle$. For clear visualization, only the vectors having length greater than the mean vector length are shown in Figure 10.

In parts a−d of Figure10, we have shown the projections of $\langle\vec{\mu}\ \rangle$ in the *xz* plane for systems 1−4. The most noticeable feature of the SOF slices in the *xz* plane is the strong inward orientation of water dipoles toward benzene center for all the systems. The projections of $\langle\vec{\mu}\ \rangle$ in the *xy* plane for system 1 are shown in Figure 10e. The orientational ordering is found to be less pronounced in this region. The tangential and outward orientations of $\langle\vec{\mu}\ \rangle$ are found to be more probable. The outward and tangential orientations of $\langle\vec{\mu}\ \rangle$ in the equatorial regions seem to appear because of the influence of the positive charge of benzene hydrogens and to maintain hydrogen bonding configurations to the water molecules present axial to the benzene ring. The SOFs in the *xy* plane show more random orientations for systems 2−4 and also for system 5 which has the same density as the ambient system but a supercritical temperature of 673 K, however the outward orientation of $\langle\vec{\mu}\ \rangle$ seems to persist to some extent even at higher temperatures (Figure 10f−h and Figure S7).

4. SUMMARY AND CONCLUSIONS

We have carried out molecular dynamics calculations to study the spatially and orientationally resolved solvation structure of a benzene molecule in liquid water of density 1.0 g cm^{-3} at 298 K and 0.87 g cm^{-3} at 473 K and also in three systems of supercritical water of densities 0.7, 0.35, and 1.0 g cm^{-3} at 673 K. The results of the benzene solvation structure of the sub- and supercritical systems have been compared with those at the ambient temperature of 298 K. The water molecules in the axial region of benzene solvation shell are found to have preferred orientation toward the benzene ring, while water molecules in the equatorial region show dipolar orientations typical of a hydrophobic surface. The πH-bonding is to exist to some extent even at supercritical conditions. This indicates that the structure of the axial regions of the solvation shell is mostly influenced by the O−H···πHB, whereas the structure of the solvation shell in the equatorial region is mostly determined by the hydrophobic interactions of water with the benzene molecule. Overall, a weakening of the hydration shell around benzene, as revealed by the reduced height of the first peak of radial distribution functions between the center of mass of benzene and oxygen atoms of water, is observed with increase in temperature and also with decrease in density at supercritical temperature. Regarding spatial range of the anisotropic solvation shell of benzene solute, an expansion of the πH-bonded part in the axial region and a contraction of the hydrophobically solvated part in the equatorial region are found as the temperature is increased from 298 K to the supercritical temperature of 673 K. The contraction of the hydrophobically solvated part in the equatorial region is found to similar to that found for the temperature dependence of the solvation shell of a purely hydrophobic solute like methane. Thus, for the benzene solute, the πH-bonded and the hydrophobically solvated parts are found to behave in a contrasting manner as one moves to supercritical states from the ambient condition.

We note that the present study of the structural behavior of water molecules in different parts of the anisotropic hydration shell of a benzene solute dissolved in supercritical, subcritical and ambient water is based on molecular dynamics simulations using classical nonpolarizable models of water. Earlier studies based on polarizable force fields and *ab initio* molecular dynamics of benzene in ambient water[38−40] have shown that nonpolarizable models overestimate the πH-bonding along the axial direction. For example, in the current work, the height of the first peak of the Bz−O correlation for the 20° axial region is found to be about 6 which agrees well with that reported in ref.[38] for the nonpolarizable TIP4P model[78] of water whereas the height of the same peak was found to be substantially less in *ab initio* simulations.[39,40] For the Bz−H correlation for the same axial region, the present study produced a higher first peak than the second one which is again in agreement with previous results for benzene in TIP4P water[38] but differs from the results of *ab initio* simulations which produced a relatively smaller first peak than the second at the ambient condition.[39,40] Thus, the nonpolarizable models of water and benzene used in the current work seem to overpredict the extent of πH-bonding along the axial direction although the extent of such overprediction, if any, at higher temperatures of sub- and supercritical water is not clear at present in view of the absence of any *ab initio* simulations of benzene in such nonambient aqueous systems at higher temperatures and reduced densities. Clearly, It would be worthwhile to investigate the position and orientation resolved solvation structure of benzene in supercritical water, specifically the extent of benzene−water πH-bonds, by means of *ab initio* simulations. We hope to address such a study in future.

■ ASSOCIATED CONTENT

Supporting Information

Table S1, average temperatures and root mean square deviations for systems 1−5, Figure S1, radial distribution functions for systems 1 and 5., Figure S2, benzene centre of mass−oxygen RDFs for systems 1 and 5, Figure S3, radial distribution functions between the carbon atom of methane and oxygen of water for all systems 1−5, Figures S4 and S5, radial/angular distribution functions of water position and dipole tilt angle, Figure S6, spatial distribution functions in Cartesian space for systems 1 and 5, and Figure S7, spatial orientational functions in Cartesian space for systems 1 and 5. The Supporting Information is available free of charge on the ACS Publications website at DOI: 10.1021/acs.jpcb.5b03371.

■ AUTHOR INFORMATION

Corresponding Author

*E-mail: amalen@iitk.ac.in.

Notes

The authors declare no competing financial interest.

■ ACKNOWLEDGMENTS

We thank Bikramjit Sharma and Banshi Das for useful discussions during this work. Financial support from the Department of Science and Technology (DST) and Council of Scientific and Industrial Research (CSIR), Government of India, is gratefully acknowledged.

DOI: 10.1021/acs.jpcb.5b03371
J. Phys. Chem. B 2015, 119, 8600−8612

REFERENCES

(1) Tanford, C. *The Hydrophobic Effect: Formation of Micellesand Biological Membranes*; John Wiley & Sons: New York, 1973.
(2) Ball, P. Water as an Active Constituent in Cell Biology. *Chem. Rev.* **2008**, *108*, 74−108.
(3) Chandler, D. Interfaces and the Driving Force of Hydrophobic Assembly. *Nature* **2005**, *437*, 640−647.
(4) Huang, D. M.; Chandler, D. Temperature and Length Scale Dependence of Hydrophobic Effects and Their Possible Implications for Protein Folding. *Proc. Natl. Acad. Sci. U.S.A.* **2000**, *97*, 8324−8327.
(5) Huang, X.; Margulis, C. J.; Berne, B. J. Dewetting-Induced Collapse of Hydrophobic Particles. *Proc. Natl. Acad. Sci. U.S.A.* **2003**, *100*, 11953−11958.
(6) Rasaiah, J. C.; Garde, S.; Hummer, G. Water in Nonpolar Confinement: From Nanotubes to Proteins and Beyond. *Annu. Rev. Phys. Chem.* **2008**, *59*, 713−740.
(7) Remsing, R. C.; Weeks, J. D. Dissecting Hydrophobic Hydration and Association. *J. Phys. Chem. B* **2013**, *117*, 15479−15491.
(8) Siboulet, B.; Coasne, B.; Dufreche, J. F.; Turq, P. Hydrophobic Transition in Porous Amorphous Silica. *J. Phys. Chem. B* **2011**, *115*, 7881−7886.
(9) Bhattacharyya, K. Nature of Biological Water: A Femtosecond Study. *Chem. Commun.* **2008**, *25*, 2848−2857.
(10) Bagchi, B. Water Dynamics in the Hydration Layer Around Proteins and Micelles. *Chem. Rev.* **2005**, *105*, 3197−3219.
(11) Bagchi, B. From Anomalies in Neat Liquid to Structure, Dynamics and Function in the Biological World. *Chem. Phys. Lett.* **2012**, *529*, 1−9.
(12) Choudhury, N.; Pettitt, B. M. On the Mechanism of Hydrophobic Association of Nanoscopic Solutes. *J. Am. Chem. Soc.* **2005**, *127*, 3556−3567.
(13) Choudhury, N.; Pettitt, B. M. Enthalpy-Entropy Contributions to the Potential of Mean Force of Nanoscopic Hydrophobic Solutes. *J. Phys. Chem. B* **2006**, *110*, 8459−8463.
(14) Blokzijil, W.; Engberts, J. B. F. N. Hydrophobic Effects. Opinions and Facts. *Angew. Chem., Int. Ed.* **1993**, *32*, 1545−1579.
(15) Rana, M. K.; Chandra, A. Ab Initio and Classical Molecular Dynamics Studies of the Structural and Dynamical Behavior of Water Near a Hydrophobic Graphene Sheet. *J. Chem. Phys.* **2013**, *138*, 204702.
(16) Kunieda, M.; Nakaoka, K.; Liang, Y.; Miranda, C. R.; Ueda, A.; Takahashi, S.; Okabe, H.; Matsuoka, T. Self-Accumulation of Aromatics at the Oil-Water Interface Through Weak Hydrogen Bonding. *J. Am. Chem. Soc.* **2010**, *132*, 18281−18286.
(17) Suzuki, S.; Green, P. G.; Bumgarner, R. E.; Dasgupta, S.; Goddard, W. A., III; Blake, G. A. Benzene Forms Hydrogen Bonds with Water. *Science* **1992**, *257*, 942−945.
(18) Gotch, A. J.; Zwier, T. S. Multiphoton Ionization Studies of Clusters of Immiscible Liquids. I. C_6H_6-$(H_2O)_n$, n=1,2. *J. Chem. Phys.* **1992**, *96*, 3388−3401.
(19) Pimentel, G. C.; McClellan, A. L. *The Hydrogen Bond*; W. H. Freeman: San Francisco, CA, 1960.
(20) Engdahl, A.; Nelander, B. A Matrix Isolation Study of the Benzene-Water Interaction. *J. Phys. Chem.* **1985**, *89*, 2860−2864.
(21) Zwier, T. S. The Spectroscopy of Solvation in Hydrogen-Bonded Aromatic Clusters. *Annu. Rev. Phys. Chem.* **1996**, *47*, 205−241.
(22) Pribble, R. N.; Garrett, A. W.; Haber, K.; Zwier, T. S. Resonant Ion-Dip Infrared Spectroscopy of Benzene−H_2O and Benzene−HOD. *J. Chem. Phys.* **1995**, *103*, 531−544.
(23) Gruenloh, C. J.; Carney, J. R.; Arrington, C. A.; Zwier, T. S.; Fredericks, S. Y.; Jordan, K. D. Infrared Spectrum of a Molecular Ice Cube: The S_4 and D_{2d} Water Octamers in Benzene-$(Water)_8$. *Science* **1997**, *276*, 1678−1681.
(24) Chakrabarti, P.; Bhattacharyya, R. Geometry of Nonbonded Interactions Involving Planar Groups in Proteins. *Prog. Biophys. Mol. Biol.* **2007**, *95*, 83−137.
(25) Steiner, T.; Koellner, G. Hydrogen Bonds with π-Acceptors in Proteins: Frequencies and Role in Stabilizing Local 3D Structures. *J. Mol. Biol.* **2001**, *305*, 535−557.
(26) Perera, P. N.; Fega, K. R.; Lawrence, C.; Sundstrom, E. J.; Tomlinson-Phillips, J.; Ben-Amotz, D. Observation of Water Dangling OH Bonds Around Dissolved Nonpolar Groups. *Proc. Natl. Acad. Sci. U.S.A.* **2009**, *106*, 12230−12234.
(27) Tassaing, T. A. Vibrational Spectroscopic Study of Water Confined in Benzene From Ambient Conditions up to High Temperature and Pressure. *Vib. Spectrosc.* **2000**, *24*, 15−28.
(28) Furutaka, S.; Ikawa, S.-I. Infrared Study of Water-Benzene Mixtures at High Temperatures and Pressures. *J. Phys.: Condens. Matter* **2002**, *14*, 11467−11475.
(29) Furutaka, S.; Ikawa, S.-I. π-Hydrogen Bonding Between Water and Aromatic Hydrocarbons at High Temperatures and Pressures. *J. Chem. Phys.* **2002**, *117*, 751−755.
(30) Kometani, N.; Takemiya, K.; Yonezawa, Y.; Amita, F.; Kajimoto, O. UV Spectral Shift of Benzene in Sub- and Supercritical Water. *Chem. Phys. Lett.* **2004**, *394*, 85−89.
(31) Gierszal, K. P.; Davis, J. G.; Hands, M. D.; Wilcox, D. S.; Slipchenko, L. V.; Ben-Amotz, D. π-Hydrogen Bonding in Liquid Water. *J. Phys. Chem. Lett.* **2011**, *2*, 2930−2933.
(32) Linse, P. Molecular Dynamics Simulation of a Dilute Aqueous Solutionof Benzene. *J. Am. Chem. Soc.* **1990**, *112*, 1744−1750.
(33) Laaksonen, A.; Stilbs, P.; Wasylishen, R. E. Molecular Motion and Solvation of Benzene in Water, Carbon Tetrachloride,Carbon Disulfide and Benzene: A Combined Molecular Dynamics Simulationand Nuclear Magnetic Resonance Study. *J. Chem. Phys.* **1998**, *108*, 455−468.
(34) Schravendijk, P.; van der Vegt, N. F. A. From Hydrophobic to Hydrophilic Solvation: An Application to Hydration of Benzene. *J. Chem. Theory Comput.* **2005**, *1*, 643−652.
(35) Lopes, P. E.; Lamoureux, G.; Roux, B.; Mackerell, A. D., Jr. Polarizable Empirical Force Field for Aromatic Compounds Based on the Classical Drude Oscillator. *J. Phys. Chem. B* **2007**, *111*, 2873−2885.
(36) Raschke, T. M.; Levitt, M. Nonpolar Solutes Enhance Water Structurewithin Hydration Shells While Reducing Interactions between Them. *Proc. Natl. Acad. Sci. U.S.A.* **2005**, *102*, 6777−6782.
(37) Raschke, T. M.; Levitt, M. Detailed Hydration Maps of Benzene and Cyclohexane Reveal Distinct Water Structures. *J. Phys. Chem. B* **2004**, *108*, 13492−13500.
(38) Mateus, M. P. S.; Galamba, N.; Cabral, B. J. C. Structure and Electronic Properties of a Benzene-Water Solution. *J. Chem. Phys.* **2012**, *136*, 014507.
(39) Allesch, M.; Schwegler, E.; Galli, G. Structure of Hydrophobic Hydration of Benzene and Hexafluorobenzene from First Principles. *J. Phys. Chem. B* **2007**, *111*, 1081−1089.
(40) Allesch, M.; Lightstone, F. C.; Schwegler, E.; Galli, G. First Principles and Classical Molecular Dynamics Simulationsof Solvated Benzene. *J. Chem. Phys.* **2008**, *128*, 014501.
(41) Linse, P.; Karlström, G.; Jönsson, B. Monte Carlo Studies of a Dilute Aqueous Solution of Benzene. *J. Am. Chem. Soc.* **1984**, *106*, 4096−4102.
(42) Ravishanker, G.; Mehrotra, P. K.; Mezei, M.; Beveridge, D. L. Aqueous Hydration of Benzene. *J. Am. Chem. Soc.* **1984**, *106*, 4102−4108.
(43) Jorgensen, W. L.; Laird, E. R.; Nguyen, T. B.; Tiradorives, J. Monte Carlo Simulations of Pure Liquid Substituted Benzenes with OPLS Potential Functions. *J. Comput. Chem.* **1993**, *14*, 206−215.
(44) Urahata, S.; Cautinho, K.; Canuto, S. Hydrophobic Interaction and Solvatochromic Shift of Benzene in Water. *Chem. Phys. Lett.* **1997**, *274*, 269−274.
(45) Urahata, S.; Canuto, S. Monte Carlo Study of the Temperature Dependence of the Hydrophobic Hydration of Benzene. *Chem. Phys. Lett.* **1999**, *313*, 235−240.
(46) Plugatyr, A.; Nahtigal, I.; Svishchev, I. M. Spatial Hydration Structures and Dynamics of Phenolin Sub- and Supercritical Water. *J. Chem. Phys.* **2006**, *124*, 024507.
(47) Plugatyr, A.; Svishchev, I. M. The Hydration of Aniline: Analysis of Spatial Distribution Functions. *J. Chem. Phys.* **2009**, *130*, 114509.

DOI: 10.1021/acs.jpcb.5b03371
J. Phys. Chem. B 2015, 119, 8600−8612

(48) Svishchev, I. M.; Plugatyr, A.; Nahtigal, I. G. Spatial Hydration Maps and Dynamics of Naphthalene in Ambientand Supercritical Water. *J. Chem. Phys.* **2008**, *128*, 124514.
(49) Koneshan, S.; Rasaiah, J. C. Computer Simulation Studies of Aqueous Sodium Chloride Solutions at 298 and 683 K. *J. Chem. Phys.* **2000**, *113*, 8125−8137.
(50) Rasaiah, J. C.; Noworyta, J. P.; Koneshan, S. Structure of Aqueous Solutions of Ions and Neutral Solutes at Infinite Dilution at a Supercritical Temperature of 683 K. *J. Am. Chem. Soc.* **2000**, *122*, 11182−11193.
(51) Nowortya, J. P.; Koneshan, S.; Rasaiah, J. C. Dynamics of Aqueous Solutions of Ions and Neutral Solutes at Infinite Dilution at a Supercritical Temperature of 683 K. *J. Am. Chem. Soc.* **2000**, *122*, 11194−11202.
(52) Fedotova, M. V. Structural Features of Concentrated Aqueous NaCl Solution in the Sub- and Supercritical State at Different Densities. *J. Mol. Liq.* **2008**, *143*, 35−41.
(53) Mallik, B. S.; Chandra, A. Vibrational Spectral Diffusion in Supercritical D_2O from First Principles: An Interplay Between the Dynamics of Hydrogen Bonds, Dangling OD Groups, and Inertial Rotation. *J. Phys. Chem. A* **2008**, *112*, 13518−13527.
(54) Mallik, B. S.; Chandra, A. An Ab Initio Molecular Dynamics Study of Supercritical Aqueous Ionic Solutions: Hydrogen Bonding, Rotational Dynamics and Vibrational Spectral Diffusion. *Chem. Phys.* **2011**, *387*, 48−55.
(55) Ohmori, T.; Kimura, Y. Anomaly of the Temperature Dependence of the Diffusion of Oxygen in Supercritical Water. *J. Chem. Phys.* **2002**, *116*, 2680−2683.
(56) Ohmori, T.; Kimura, Y. Translational Diffusion of Hydrophobic Solutes in Supercritical Water Studied by Molecular Dynamics Simulations. *J. Chem. Phys.* **2003**, *119*, 7328−7334.
(57) Nieto-Draghi, C.; Avalos, J. B.; Contreras, O.; Ungerer, P.; Ridard, J. Dynamical and Structural Properties of Benzene in Supercritical Water. *J. Chem. Phys.* **2004**, *121*, 10566−10576.
(58) Mallik, B. S.; Chandra, A. Hydrogen Bond and Residence Dynamics of Ion-Waterand Water-Water Pairs in Supercritical Aqueous Ionic Solutions: Dependence on Ion Size and Density. *J. Chem. Phys.* **2006**, *125*, 234502.
(59) Jorgensen, W. L.; Maxwell, D. S.; Tirado-Rives, J. Development and Testing of the OPLS All-Atom Force Fieldon Conformational Energetics and Properties of Organic Liquids. *J. Am. Chem. Soc.* **1996**, *118*, 11225−11236.
(60) Berendsen, H. J. C.; Grigera, J. R.; Straatsma, T. P. The Missing Term in Effective Pair Potentials. *J. Phys. Chem.* **1987**, *91*, 6269−6271.
(61) See the Supporting Information available online with this article for properties of system 5. The results of the same-density system at ambient condition (system 1) are also included in the Supporting Information for the purpose of comparison. Besides, tables containing the results of average temperatures and the associated root-mean-square deviations for systems 1−5 during the production phases of the simulation runs are also included in the Supporting Information.
(62) Allen, M. P.; Tildesley, D. J. *Computer Simulation of Liquids*; Oxford University Press: New York, 1987.
(63) Rana, M. K.; Chandra, A. Wetting Behavior of Nonpolar Nanotubes in Simple Dipolar Liquids for Varying Nanotube Diameter and Solute-Solvent Interactions. *J. Chem. Phys.* **2015**, *142*, 34704.
(64) Rana, M. K.; Chandra, A. Solvation Structure of Nanoscopic Hydrophobic Solutes in Supercritical Water: Results for Varying Thickness of Hydrophobic Walls, Solute-Solvent Interaction and Solvent Density. *Chem. Phys.* **2012**, *408*, 28−35.
(65) Gupta, R.; Chandra, A. Nonideality in Diffusion of Ionic and Neutral Solutes and Hydrogen Bond Dynamics in Dimethyl Sulfoxide-Chloroform Mixtures of Varying Composition. *J. Comput. Chem.* **2011**, *32*, 2679−2689.
(66) Paul, S.; Chandra, A. Structure, Dynamics and the Free Energy of Solute Adsorption at Liquid-Vapor Interfaces of Simple Dipolar Systems: Molecular Dynamics Results for Pure and Mixed Stockmayer Fluids. *J. Phys. Chem. B* **2007**, *111*, 12500−12507.
(67) Chowdhuri, S.; Chandra, A. Hydrogen Bonds in Aqueous Electrolyte Solutions: Statistics and Dynamics Based on Both Geometric and Energetic Criteria. *Phys. Rev. E* **2002**, *66*, 041203−041207.
(68) Chowdhuri, S.; Chandra, A. Dynamics of Ionic and Hydrophobic Solutes in Water-Methanol Mixtures of Varying Composition. *J. Chem. Phys.* **2005**, *123*, 234501.
(69) Chandra, A.; Ichiye, T. Dynamical Properties of the Soft Sticky Dipole Model of Water: Molecular Dynamics Simulations. *J. Chem. Phys.* **1999**, *111*, 2701−2709.
(70) Wallen, S. L.; Palmer, B. J.; Pfund, D. M.; Fulton, J. L.; Newville, M.; Ma, Y.; Stern, E. A. Hydration of Bromide Ion in Supercritical Water: An X-ray Adsorption Fine Structureand Molecular Dynamics Study. *J. Phys. Chem. A* **1997**, *101*, 9632−9640.
(71) Balbuena, P. B.; Johnston, K. P.; Rossky, P. J. Molecular Dynamics Simulation of Electrolyte Solutions in Ambient and Supercritical Water. 1. Ion Solvation. *J. Phys. Chem.* **1996**, *100*, 2706−2715.
(72) Morita, A.; Hynes, J. T. A Theoretical Analysis of the Sum Frequency Generation Spectrum of the Water Surface. *Chem. Phys.* **2000**, *258*, 371−390.
(73) Mecke, M.; Winkelmann, J.; Fischer, J. Molecular Dynamics Simulation of the Liquid-Vapor Interface: The Lennard-Jones Fluid. *J. Chem. Phys.* **1997**, *107*, 9264−9270.
(74) Ghorai, P. K.; Yashonath, S. Evidence in Support of Levitation Effect as the Reason for Size Dependence of Ionic Conductivity in Water: A Molecular Dynamics Simulation. *J. Phys. Chem. B* **2006**, *110*, 12179−12190.
(75) Mateus, M. P. S.; Galamba, N.; Cabral, B. J. C.; Coutinho, K.; Canuto, S. Electronic Properties of a Methane-Water Solution. *Chem. Phys. Lett.* **2011**, *506*, 183−189.
(76) Kusalik, P. G.; Svishchev, I. M. The Spatial Structure in Liquid Water. *Science* **1994**, *265*, 1219−1221.
(77) Svishchev, I. M.; Kusalik, P. G. Structure in Liquid Water: A Study of Spatial Distribution Functions. *J. Chem. Phys.* **1993**, *99*, 3049−3058.
(78) Jorgensen, W. L.; Chandrasekhar, J.; Madura, J. D.; Impey, R. W.; Klein, M. L. Comparison of Simple Potential Functions for Simulating Liquid Water. *J. Chem. Phys.* **1983**, *79*, 926−935.

DOI: 10.1021/acs.jpcb.5b03371
J. Phys. Chem. B 2015, 119, 8600−8612